Vertical Upward Cocurrent Gas-Liquid Annular Flow

Upward cocurrent gas-liquid annular flow was investigated in a 50.8 mm ID cylindrical vertical pipe. The film flow was studied by measuring instantaneous local film thickness, wall shear stress, and pressure gradient. Analysis of these data revealed that at low gas flow rates the film motion is controlled by a switching mechanism, as speculated by Moalem-Maron and Dukler (1984). In the region of high gas flow rates the switching process is suppressed and traveling roll waves characterize the film motion.

G. Zabaras and A. E. Dukler
University of Houston
Houston, TX 77004

D. Moalem-Maron
Faculty of Engineering
Tel-Aviv University
Tel-Aviv, Israel

SCOPE

Vertical upward cocurrent gas-liquid annular flow exists in a wide variety of industrial processes such as production and pipeline systems for offshore delivery of oil and gas; emergency core cooling facilities for protection of nuclear reactors in the event of a loss-of-coolant accident; process equipment for gas-liquid contacting and reaction; and high-capacity geothermal wells with associated surface equipment.

A variety of empirical or semiempirical correlations have been proposed for predicting such characteristics as pressure drop (Orkiszewski, 1967; Wallis, 1969) and equilibrium rates of entrainment (Whalley and Hewitt, 1978). However, the predictions are not reliable at conditions different from those of the experiments used to construct the correlations. The pressure-gradient in annular flow is much higher than for turbulent gas flow in a smooth pipe. A number of relationships have been proposed for interfacial shear, but these correlations do not give reliable predictions outside the range for which they were originally derived. Thus the need exists for an understanding of the basic physical processes taking place in order to be able to construct sound, mechanistically based models. In a recent theoretical study, Moalem-Maron and Dukler (1984) suggested that the variation of the thickness of the liquid film resulted from a process of switching between unstable steady state solutions to the equation of motion rather than to the motion of roll and capillary waves along the surface. This paper reports on new measurements and an interpretation to test this idea.

CONCLUSIONS AND SIGNIFICANCE

Experimental data have been obtained for vertical upward cocurrent annular gas-liquid flow. These include local instantaneous film thickness, direction and magnitude of the wall shear stress, and pressure gradient. Analysis of the data in a variety of ways suggests that at low gas flow rates the motion of the interface is controlled by a process of switching between possible steady states of the system as described by Moalem-Maron and Dukler (1984). This condition is usually designated as churn flow, but bridging of the liquid across the pipe as associated with churning does not take place. This switching process can be expected to be accompanied by large dissipative effects. Modeling of the mixing processes associated with heat or mass transfer must be based on the dynamics of switching rather than on wave motion.

At high gas flow rates the interface is characteristic of a sequence of traveling roll waves as described by others. The switching is suppressed.

Introduction

A robust literature now exists dealing with upward gas-liquid annular film flow in vertical tubes. The high publication rate in recent years has been driven by the need for reliable methods to design and predict performance of large, high capital cost installations that must operate with a high degree of predictability. Empirically based correlations now available for such quantities as pressure gradient, entrainment, or heat and mass transfer rates have been found to be reliable only at conditions near the data from which they were built. The need exists to understand the basic mechanisms controlling the flow so that physically sound models can be constructed. However, studies that reveal these basic mechanisms are few in number. Data on the properties of the mean motion such as film thickness, pressure gradient, and entrainment have been reported (Lacey and Hewitt, 1962; Whalley et al., 1973; Malafeev et al., 1976; Subbotin et al, 1978). The particular behavior of disturbance waves has been examined (Hall-Taylor and Nedderman, 1968; Nedderman and Shearer, 1963), as has the statistical nature of the wavy interface (Tomida and Okazaki, 1974; Nikolaev et al., 1975; Kvurt, 1978; Smith et al., 1984). Despite careful planning of experiments and data collection, no significant insights into mechanisms seem to have emerged from this work.

The pressure gradient is substantially higher than would exist for flow across a smooth interface. Measurements of pressure gradient across a solid wavy surface similar in size and shape to the large waves on the interface give much lower values than observed during annular flow (Kennedy and Hsu, 1971; Zielker and Hanratty, 1979; Buckles et al., 1984). Treating the small waves as a rough solid surface requires unrealistically large equivalent roughnesses to account for the observed interfacial shear. Again, there appears to be a lack of understanding of the underlying mechanisms. The enhanced momentum transfer seems to be due to the presence of the mobile interface. This wavy interface can also account for increased rates of mass transfer as described by Dukler (1977).

Nicklin and Koch (1969), suggested that annular flow could be visualized as a condition of incipient flooding with the surface film thickness assuming the value necessary to satisfy the momentum balance between the wall shear and gravity. As the film thickness changes due to random variation, the interfacial shear adjusts to maintain the value needed to support the film. This early attempt at understanding the underlying mechanism was elaborated in a theoretical analysis by Moalem-Maron and Dukler (1984) which explored film mechanisms for both flooding and upward cocurrent annular flow. This paper represents an extension and test of those ideas.

A Steady State Model for Film Flow

Consider a liquid film uniformly introduced on the inner wall of a vertical tube at a location somewhere along its length. Gas flows upward. At the flooding condition, liquid first appears above the feed and a sharp increase in pressure gradient is observed there. As the gas flow rate is increased the fraction of feed flowing upward increases until a point is reached where all the liquid flows upward. Further increases in gas flow rate result in thinner films and higher velocities but the mass flow rate remains the same.

The pressure gradient decreases with increasing gas flow rate, and at some point it displays a minimum, as has been demonstrated by Hewitt et al. (1965). Operating conditions between the flooding point and the point of minimum pressure gradient are frequently designated as churn flow. The liquid film structure appears to be completely different on either side of the pressure drop minimum. At gas rates above the minimum ΔP, experimental studies by Hall-Taylor et al. (1963) and by Hall-Taylor and Nedderman (1968) revealed the existence of large disturbance waves propagating upwards. Hewitt et al. (1965) suggested that the point of minimum pressure drop corresponds to the condition at which the wall shear stress τ_w is zero. Hewitt (1982) also speculated that at high gas flow rates the wall shear stress fluctuates around a negative (directed downward) mean value but never changes sign, while in the region below the minimum pressure gradient the wall shear stress fluctuates around zero, taking both negative and positive values. No experimental data were advanced to test these speculations, but strong support came from a recent theoretical study of the film flow mechanism by Moalem-Maron and Dukler (1984). These authors start their analysis by considering the equation for steady, laminar, one-dimensional motion of an incompressible, Newtonian fluid; that is

$$\nu_L = \frac{\partial^2 u}{\partial y^2} + \phi g = 0 \tag{1}$$

where

$$\phi = \frac{g - \frac{1}{\rho_L}\frac{dP}{dx}}{g}. \tag{2}$$

Equation 1 was solved for a smooth film. This was equivalent to the assumption that the effect of the wave motion on the velocity in the film averages out over position and time. The boundary conditions were

$$u = 0 \quad \text{at} \quad y = 0 \tag{3}$$

$$-\mu \frac{\partial u}{\partial y} = \tau_i \quad \text{at} \quad y = \delta. \tag{4}$$

In Eq. 4 τ_i represents the interfacial shear stress.

The solution of Eq. 1 yields the following velocity distribution

$$u = \frac{\rho_L \phi g}{\mu_L}\left[\left(\delta - \frac{\tau_i}{\rho_L g \phi}\right)y - \frac{y^2}{2}\right]. \tag{5}$$

When the film thickness is such that $\tau_i = \rho_L g \phi \delta$ the shear stress at the wall is zero. At this condition the shear stress fully supports the weight of liquid film. Designate this thickness as δ_u and the condition as the U state. Note from Eq. 5 that when $\delta > \delta_u$ the velocity near the wall is positive (or directed downward) while the flow is upward for larger values of y and is therefore negative. This implies a form of internal recycle in the film. On the other hand, when $\delta < \delta_u$ the velocity is uniformly negative for all y, flowing upward at all positions in the film. Integration of the velocity over the film thickness, δ, yields

$$Q_L = \frac{\rho_L \phi g \delta^3}{3\mu_L}\left[1 - \frac{3}{2}\frac{\tau_i}{\rho_L \phi g \delta}\right]. \tag{6}$$

Since for upflow $Q_L = -Q_F$, Eq. 6 becomes

$$\delta^3 - \frac{3}{2}\frac{\tau_i}{\rho_L \phi g}\delta^2 + \frac{3Q_F\mu_L}{\rho_L \phi g} = 0. \tag{7}$$

The last term in Eq. 7 is δ_N^3/ϕ where δ_N is the Nusselt film thickness that corresponds to a free falling film at the same flow rate. Normalizing δ by δ_N then yields this result:

$$R_N^3 - \frac{3}{2}GR_N^2 + \frac{1}{\phi} = 0 \tag{8}$$

where

$$R_N = \delta/\delta_N \quad G = \frac{\tau_i}{\rho_L \phi g \delta_N}. \tag{9}$$

Equation 8 can be shown to have three real roots, one of which is negative and thus nonphysical. Also, in most practical cases the pressure gradient is negligible compared with $\rho_L g$ and thus $\phi \to 1.0$. The solution to Eq. 8 for $\phi \approx 1.0$ appears in Figure 1 as a function of the dimensionless interfacial shear parameter G. The branch EU of the solution represents uniform upflow and the branch UC is upflow circulation. The branch point U represents the U state, which corresponds to zero wall shear stress.

The theoretical expression for the wall shear stress can be derived from Eq. 5 and is given by

$$\frac{\tau_w}{\tau_{wN}} = R_N - G \tag{10}$$

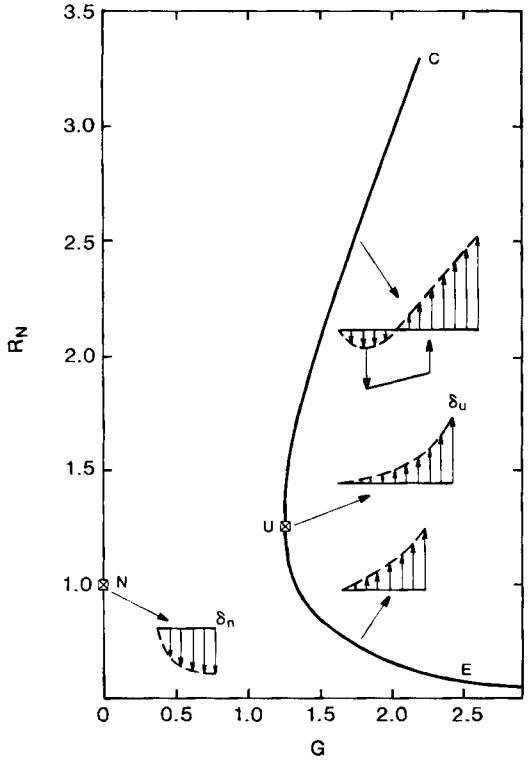

Figure 1. Variation of dimensionless film thickness with dimensionless interfacial shear stress.

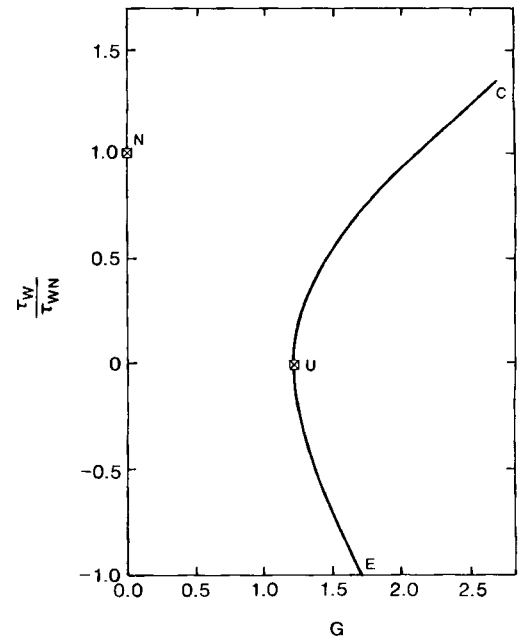

Figure 2. Variation of dimensionless wall shear stress with dimensionless interfacial shear stress.

for $\phi = 1.0$. τ_{wN} is the wall shear stress for a smooth free falling film and is equal to

$$\tau_{wN} = \rho_L g \delta_N. \tag{11}$$

Figure 2 displays the ratio τ_w/τ_{wN} as a function of the parameter G. There are again two branches, of which UE corresponds to negative wall shear (uniform upflow) and CU to positive wall shear (upflow circulation).

A comparison of measured mean film thicknesses of Smith et

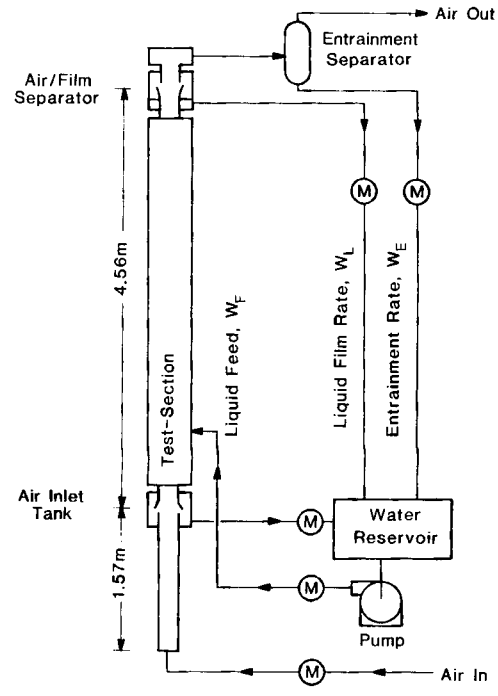

Figure 3. Schematic diagram of flow loop.

al. (1984) with this theory led Moalem-Maron and Dukler to speculate that at gas flow rates above the flooding point and below the minimum pressure gradient the film switches between the two branches of this curve. Another consequence of the theory is that over the same flow rate range the wall shear must randomly switch sign and the mean value should be between the two branches of the curve in Figure 2. Based on this speculation the dominant structure is pictured as that due to the switching between film thicknesses, which represent different states of the system, rather than due to a defined wave structure. This is in strong contrast with downward flow where the wave structure dominates (Dukler, 1977). Based on these results it became clear that careful dynamic measurements of the direction of the wall shear stress as well as its magnitude could unambiguously test this speculation as to switching. This paper reports on the development and use of a transducer for that purpose along with careful simultaneous measurements of film thickness and pressure gradient over short length so as to permit the calculation of a local value of interfacial shear stress. The combined simultaneous measurement of time-dependent values of wall shear stress, its direction, pressure gradient, and film thickness was undertaken to provide further insight into the dynamic behavior of these rising films.

Experimental

Flow loop

A schematic diagram of the flow loop is shown in Figure 3. Air, supplied by a rotary compressor, is introduced in the system through a 1.57 m long pipe of 50.8 mm ID, which is axially aligned with the test section. Liquid film flowing downward is separated from the rising stream by means of a flared section at the bottom air inlet tank. A controller maintains a constant liquid level in this tank and passes the liquid to the reservoir. At the top of the column there is a similar tank where the air/liquid film separation takes place. Another controller maintains a constant liquid level in this tank with fluid metered as it passes to the reservoir. The air stream carrying liquid droplets enters a centrifugal separator where the liquid is removed and metered to the reservoir. Liquid feed is supplied by a centrifugal pump; after passing through a calibrated rotameter it enters the system through an annulus whose inside wall consists of a porous stainless steel sinter having 100 μm pore size. As is indicated in Figure 3, in addition to the liquid and air feed flow rates, the upflow and entrainment rates are also measured.

The test section is made of transparent Plexiglass pipe of 50.8 mm ID and is shown schematically in Figure 4. A porous sinter similar to that used for the liquid feed is located near the top and is used to withdraw the major part of upward film flow, with the remainder being removed at the top tank through the flared section.

Measuring station and measuring techniques

The measuring station is shown in Figure 5. This is a 290 mm long Plexiglas tube of 50.8 mm ID. Two wall shear stress probes, two film thickness probes, and a differential pressure transducer

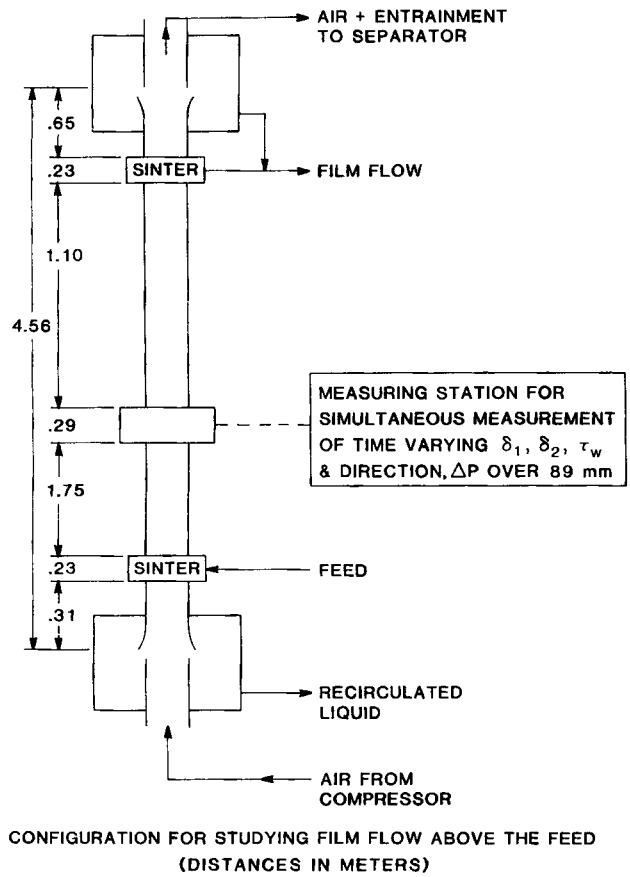

Figure 4. Configuration of test section.

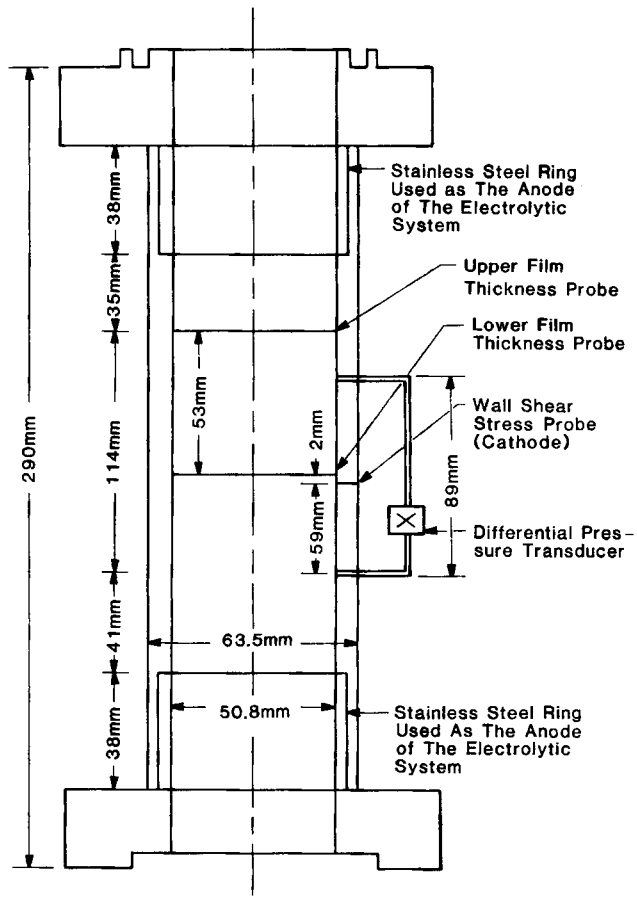

Figure 5. Measuring station.

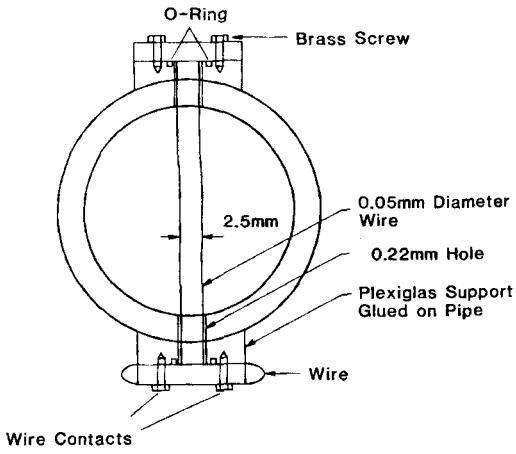

Figure 6. Film thickness probe.

are mountd on the measuring station, which can be removed from the flow loop for calibrations.

Each film thickness probe consists of two parallel platinum-13% rhodium wires 0.05 mm in dia. placed 2.5 mm apart and oriented as shown in Figure 6. As the thickness of the liquid film varies, the conductivity between the two wires changes and the fluctuations in film thickness can be transduced to voltage variations. The two wires are lacquer-insulated over one-half of their length, thus the system responds to film thickness changes on only one side of the pipe; the method is described in detail by Brown et al. (1978). An analytical solution shows that when the wires are of uniform diameter and are parallel, there exists a frequency range over which there is a linear relationship between film thickness and conductivity. In order to insure accuracy, this relationship was obtained by calibration, setting the measuring section horizonal, blocking the ends, creating a series of liquid levels whose heights were determined with a cathetometer accurate to 0.01 mm, and measuring the conductivity. A new circuit, shown in Figure 7, was designed and constructed to insure linearity between output voltage and film thickness with good frequency response to over 500 Hz.

Time-varying pressure gradient was measured over a distance of 89 mm. A Validyne variable reluctance differential pressure transducer was used and the connecting lines were filled with liquid. Care was taken to purge the liquid and bleed the lines for removal of air bubbles.

The wall shear stress measurement method is based upon the diffusion-controlled eletrolysis technique discussed by Reiss and Hanratty (1962). The local wall shear stress is shown to be related to the mass transfer coefficient of a diffusing species measured on a small, electrically isolated element of the pipe surface. The mass transfer coefficient can be determined by measuring the current flow at a small electrode embodied in the surface, using an electrochemical reaction. The small surface element forms one electrode (cathode); a much larger electrode (anode) is placed elsewhere in the system. The following redox chemical reaction is used

$$Fe(CN)_6^{3-} + e \rightarrow Fe(CN)_6^{4-} \quad \text{at the cathode}$$

$$Fe(CN)_6^{4-} \rightarrow Fe(CN)_6^{3-} \quad \text{at the anode}$$

By applying a constant voltage, within the polarization voltage range of the system used the concentration of the ferricyanide ions at the cathode surface falls to zero level and a concentration boundary layer is formed. Since the Schmidt number of the system, $\mu_L/\rho_L\mathcal{D}$ is so high ($\sim 10^3$) the thickness of the boundary layer is very small, in this case of the order of 10^{-5} m. This is well within the laminar sublayer where the velocity is linear with distance from the wall so that $u \simeq \tau_w/\mu_L\, y$. Fluctuations in shear therefore reflect velocity fluctuations in this sublayer region. When the thickness of the concentration boundary layer is small compared to the electrode width, and if the fluctuations are slow enough that the system can be considered in a condition of pseudosteady state, the convective diffusion equation reduces to

$$\frac{\tau_w}{\mu_L} y \frac{\partial c}{\partial x} = \mathcal{D} \frac{\partial^2 c}{\partial y^2} \tag{12}$$

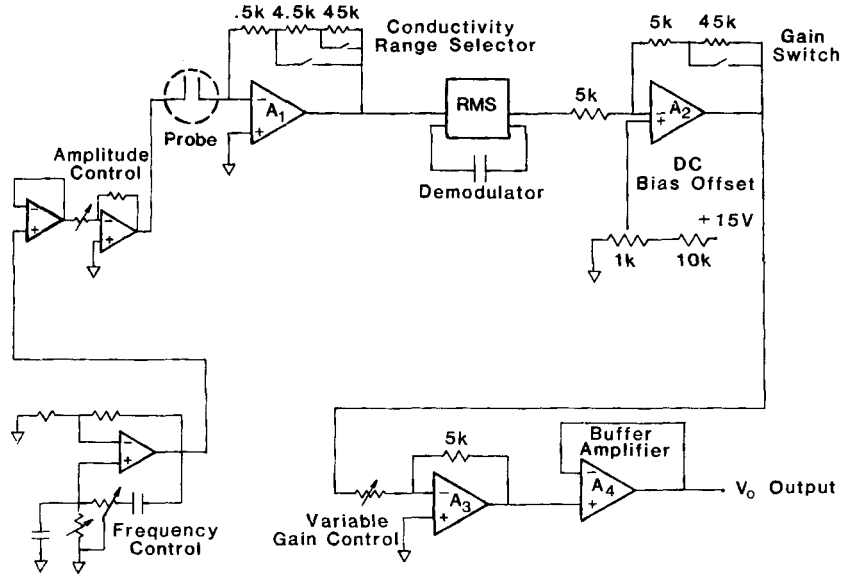

Figure 7. Conductivity monitoring circuit.

whose solution under the boundary conditions

$$y = 0 \quad c = 0 \quad \text{large } y, \quad x = 0 \quad c = c_B$$

is given by

$$k = 0.807\,\mathcal{D}\left(\frac{\tau_w}{\mu_L \mathcal{D} L}\right)^{1/3} \tag{13}$$

$$k = \frac{1}{LC_B}\int_0^L \mathcal{D}\left(\frac{\partial c}{\partial y}\right)_{y=0} dx \tag{14}$$

L is the length of the electrode in the direction of mean flow, x, and is the diffusion coefficient for the ferricyanide ions.

The technique described above only provides information on the magnitude of the shear stress with no indication of direction. A modification of this device was constructed in order to provide both. This consisted of two closely spaced cathodes aligned in the direction of the liquid flow. Each was equipped with independent circuits to measure shear stress. If both probes have identical area and the flow is in the direction from probe 1 to probe 2, the second probe will indicate a lower mass transfer rate (and wall shear stress) because its boundary layer lies in the wake of that of the first probe. When the flow changes direction the opposite is true. Thus if both probes are operated simultaneously a simple comparison of the output of the two indicates the direction. The two-probe system was first suggested by Son and Hanratty (1969) and was recently used by Cognet et al. (1984) to study gas-liquid slug flow.

A new circuit, shown in Figure 8, was developed to apply polarizing voltage and measure the current flow, which is a direct indication of the mass transfer coefficient. An output voltage was provided proportional to this current. Each electrode consisted of a curved nickel plate approximately 0.075 mm (in the flow direction) × 1 mm wide and mounted flush with the inner wall of the curved pipe so as to avoid any protrusions. The

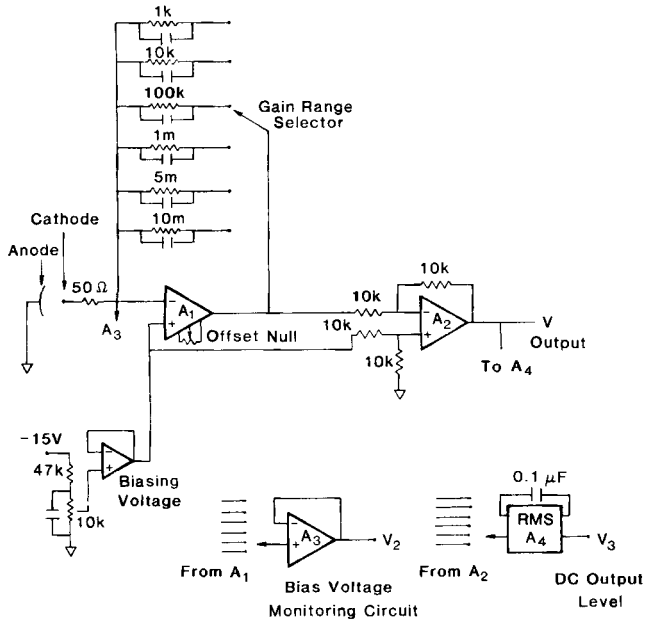

Figure 8. Wall shear stress monitoring circuit.

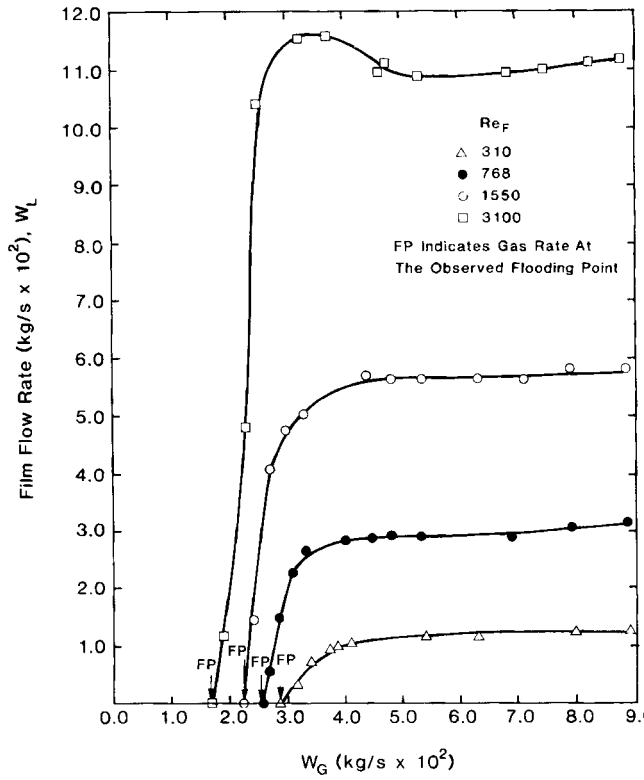

Figure 9. Liquid film flow rate.

two electrodes were separated by 0.03 mm. Calibration of the probes was accomplished by placing a solid cylindrical core concentrically located in the measuring stations (Figure 5) using a special jig, thus forming an annular gap. The gap was operated in laminar flow. The theoretical solution for annular flow was used to relate mass transfer rates as measured with the circuit and calculated wall shear stress. The general form of the relationship between τ_w and k_c given by Eq. 13 was confirmed.

Determining the direction of shear by comparing output voltages of the two probes requires that the two probes have equal area. Complications in fabrication make it impossible to accomplish this. However the relative areas can easily be determined by activating each probe individually under identical flow conditions during calibration. The ratio of the areas is equal to the measured ratio of the mass transfer coefficients.

The fluid used was a 1 M solution of sodium hydroxide together with 0.005 M potassium ferricyanide and 0.005 M

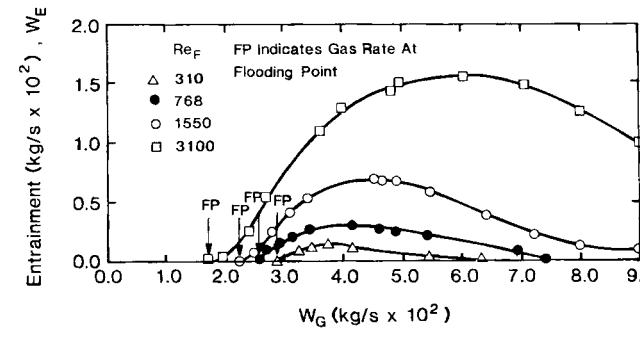

Figure 10. Entrainment rate.

potassium ferrocyanide. Values of the solution physical properties at 25°C are: density, 1,020 kg/m^3; viscosity, 0.00104 kg/ms. The surface tension of the solution was not measured, but it was thought to be much lower than that of distilled water. Brauner and Moalem-Maron (1982) report the value of 0.01 N/m for 0.01 M potassium ferricyanide and 0.01 M potassium ferrocyanide in a 1 M solution of sodium hydroxide in distilled water. The average operating air pressure of the system was 1.4 bar (140 kPa).

Data recording, digitization, storage, and processing

The two voltage signals from the two wall shear stress probes, the signals from two film thickness probes, and the signal from the differential pressure transducer were simultaneously recorded by an Ampex PR-2200 high-accuracy multichannel tape recorder. Each data set was collected over a period of less than 3 h to avoid drift of the wall shear stress calibration curve due to the effect of the dissolved oxygen. Careful calibrations were made prior to and after taking the data set, and the maximum deviation observed was of the order of 7%. This is of the order of the calibration error expected due to possible eccentricity of the annular gap in the calibration section. Thus the effect of the dissolved oxygen was tolerable for the short period over which the data set was recorded. Sutey and Knudsen (1967) found that in a 170 min period measured mass transfer coefficients for 50% oxygen saturated solution were still within 3% of the measured values for zero oxygen concentration, thus confirming these results.

The analog data were digitized by special software developed for this purpose using a PDP 11/34 minicomputer. A sampling frequency of 500 Hz was used. Signals recorded over a 2 min period for each flow condition were used for data processing. Calibration curves were applied to each signal, the area ratio was applied to the shear signals, and these normalized values compared to determine the direction of the shear. All this was done digitally.

Details as to individual units of equipment, measurement techniques, electronic instrumentation, test procedures, estimated measurement errors, and software are given by Zabaras (1985), where complete tabulations of experimental data also appear.

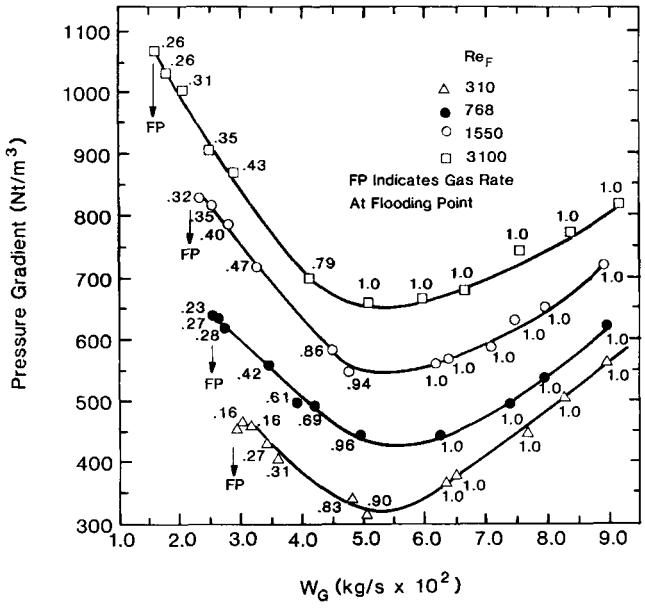

Figure 11. Average pressure gradient.

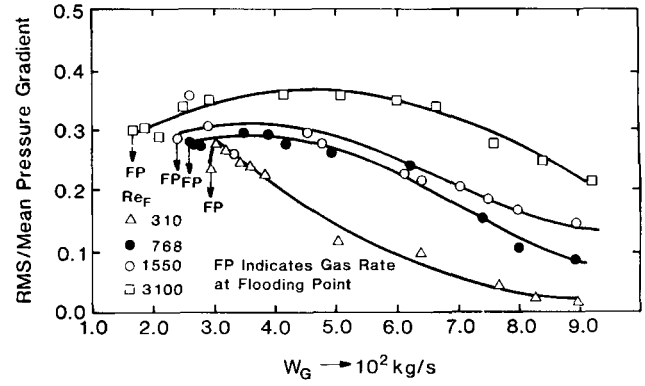

Figure 12. Ratio of RMS to mean pressure gradient.

Measurements

Liquid feed distribution

The measured liquid film flow rate, W_L, and the entrainment rate, W_E, appear in Figures 9 and 10 as functions of the gas flow rate. The entrainment curves display a maximum with gas rate. The decrease at high gas flow rates can be understood in view of the decreasing mean and RMS film thickness fluctuations as the gas rate is increased. Entrainment measurements made by Smith et al. (1984) in the same apparatus showed the same qualitative trends. However the entrainment values found were almost double those shown in Figure 10. The physical properties of the liquid in this study were different due to the use of cyanide salts and sodium hydroxide solution. A repeat of the measurements with tap water resulted in values of entrainment in close agreement with those reported by Smith.

Pressure gradient

The time-average pressure gradient measured over a distance of 89 mm is shown in Figure 11. The pressure drop displays a minimum with gas flow rate. The gas rate corresponding to this minimum is rather insensitive to the liquid rate and corresponds approximately to a dimensionless gas velocity $V_G^* = 1.06$ where

$$V_G^* = \bar{V}_G \rho_G^{1/2} [gD(\rho_L - \rho_G)]^{-1/2} \qquad (15)$$

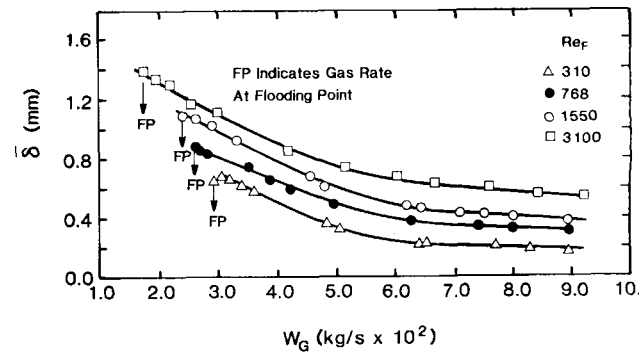

Figure 13. Mean film thickness.

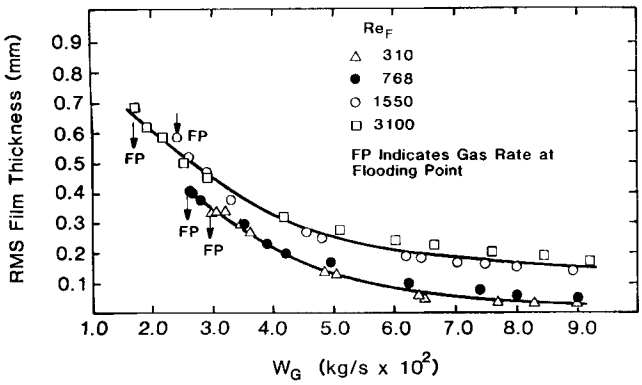

Figure 14. RMS fluctuation of film thickness.

Similar trends in the pressure gradient have been observed by Hewitt et al. (1965), who report a value of $V_G^* = 1.12$ for the gas velocity at the minimum pressure-drop point. The region to the left of the minimum has been designated churn flow, implying the process of bridging of liquid across the pipe. The region to the right of the minimum has been designated annular dispersed flow. Figure 12 shows the ratio of the RMS fluctuation to the mean pressure gradient. In contrast with the pressure gradient, the fluctuations in the pressure gradient are at a maximum close to the point of initiation of upward flow.

Film thickness

Time-average film thickness values are plotted in Figure 13. Film thickness is seen to be maximum just at the flooding point and to decrease for increasing gas flow rate. A similar trend is shown by the RMS fluctuations in film thicknesses shown in Figure 14. Near flooding the fluctuation in film thickness can be as much as 50% of the mean. Of particular interest are the data shown in Figure 15 representing the maximum film thickness. Each point corresponds to the average of the ten largest single values of film thickness found in a 2 min digitized time trace. Observe that under no condition does the maximum thickness approach the radius of the pipe. Despite the fact that bridging has been suggested as the condition that exists at gas flow rates below that for the minimum pressure drop, the data of Figure 15 show that the film thickness never exceeds 20% of the radius of the pipe.

Comparison with the data of Smith et al. (1984) shows that the values of mean thickness are approximately 25% larger at

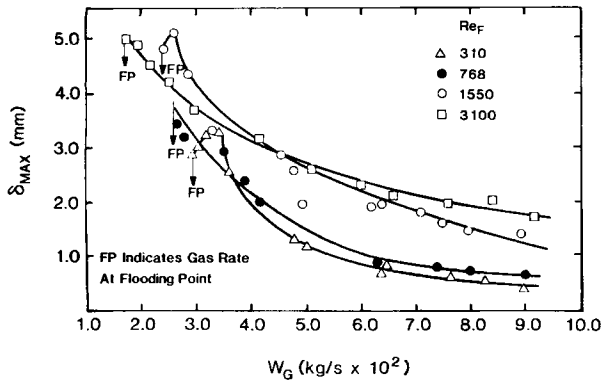

Figure 15. Maximum film thickness.

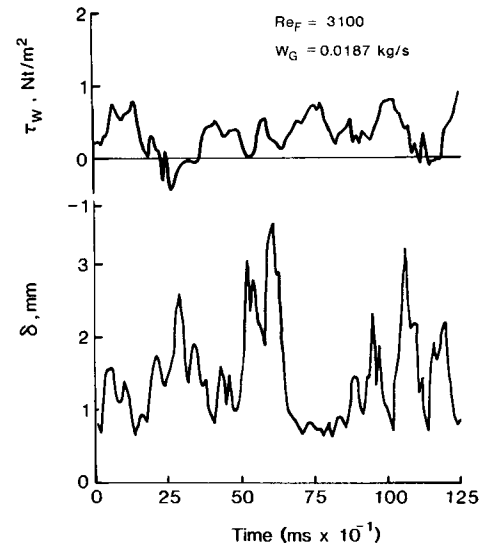

Figure 16. Simultaneous wall shear stress and film thickness traces for a condition close to the flooding point.

conditions close to the flooding point but deviate less at higher gas flow rates. The different physical properties of the liquid used in this work plus the fact that a nonlinear film thickness probe was used by Smith et al. can account for these differences.

Wall shear stress

Figure 16 shows typical simultaneous local traces of wall shear stress and film thickness. These traces correspond to a flow condition close to flooding. At this flow condition the wall shear stress switches sign, as had been speculated by Moalem-Maron and Dukler, thus implying that the solution of the flow equation switches between branch *UC* and *UE* of Figure 1. Note that little or no correlation exists between the shear and the film thickness. In this figure negative τ_w indicates downward direction, corresponding to upflow near the wall. Figure 17 represents simultaneous recordings of film thickness and wall shear stress at a gas flow rate much higher than that for the minimum pressure drop. In this case the shear is always negative, the film is in the state of uniform upflow at all times (branch *UE*), and

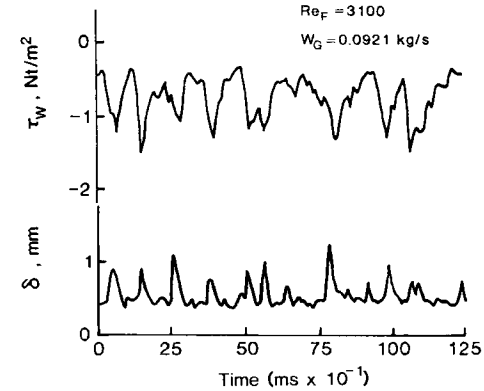

Figure 17. Simultaneous wall shear stress and film thickness traces for a high gas flow rate condition.

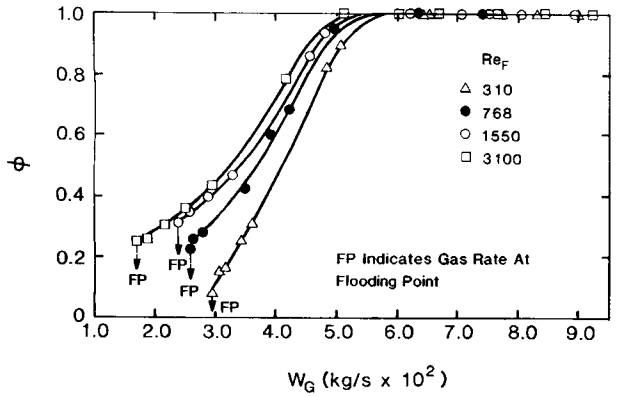

Figure 18. Fraction of time wall shear stress is directed downward.

switching does not take place. Excellent correlation exists between film thickness and wall shear stress.

The data were analyzed to determine the fraction of time the shear stress is directed downward; the result appears in Figure 18. These numerical values are shown for each data point of Figure 11. It becomes clear that the region to the left of the minimum is one where the film experiences switching between possible states and that the region to the right is the state of uniform upflow. Both are annular flow, in contrast to previous speculations on the existence of churn flow. The process of switching accounts for the chaotic appearance of this state rather than bridging of the fluid across the tube.

Figure 19 compares the measured time-average pressure gradient with the time-average gravitational contribution to the pressure drop, computed from the measured time-average film thickness. Close to the flooding point, where switching takes place, the pressure gradient due to hydrostatics is somewhat higher than the total measured value. There must therefore be a compensating force acting at the wall directed upward. Thus although the mean flow in the liquid film is directed upward, there exists a wall shear also directed upward and the flow adjacent to the wall must be downward-directed. This is precisely the situation of upflow circulation corresponding to solution branch *UC* shown in Figure 1.

As the gas flow rate increases a point of exact balance between measured gradient and that due to gravity is reached, indicating that the wall shear is zero. The data in Figure 19 suggest that this does not occur at flow condition for the minimum pressure gradient. Direct measurement of wall shear stress is reported below. As the gas flow rate is increased, the shear stress at the wall changes direction and assumes an increasing role in balancing the interfacial shear, while the gravitational contribution decreases.

Designate as *A, B, C, D, F, G, H, K* seven experimental conditions along the pressure gradient curve for the liquid Reynolds number $Re_F = 768$, Figure 20. For this sequence of flow conditions wall shear stress traces are shown in Figures 21 and 22. At gas flow rates ranging from the flood condition to the point of minimum pressure gradient, the wall shear stress switches randomly between positive and negative values with the mean value gradually moving from positive (directed upward) to a small negative value. As the minimum pressure-drop point is approached the wall shear stress fluctuations become of smaller amplitude. Further increases in gas flow rate beyond the minimum pressure drop cause the film to move to a condition of upflow, and switching of the τ_w stops.

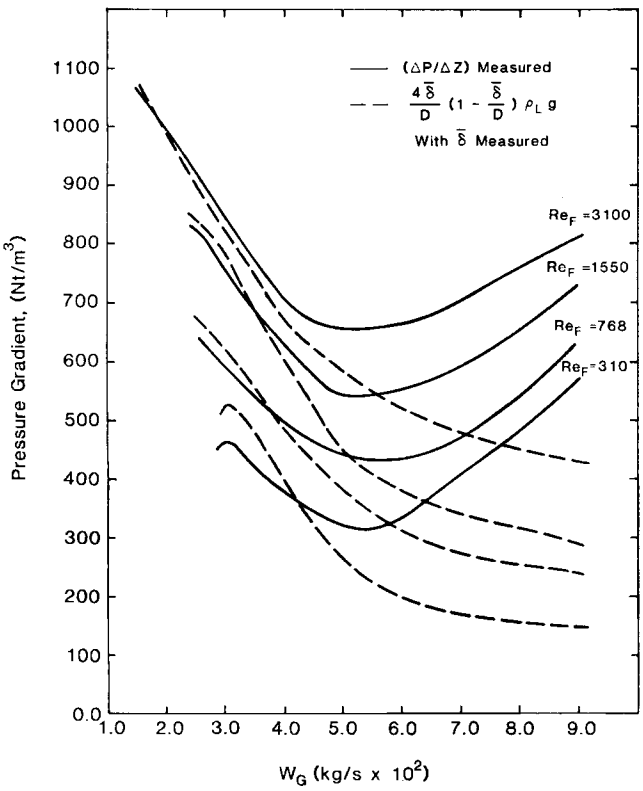

Figure 19. Total pressure gradient and its gravitational contribution.

Interpretation of the Data

Figure 23 presents, in dimensional coordinates, the variation of film thickness with interfacial shear stress as predicted by the switching theory discussed earlier. Experimental values of the mean film thickness vs. the mean interfacial shear stress, τ_i, appear as data points. The interfacial shear stress was calculated from the measured pressure gradients by the equation

$$\tau_i = -\frac{dP}{dx}\frac{D-2\delta}{4} \tag{16}$$

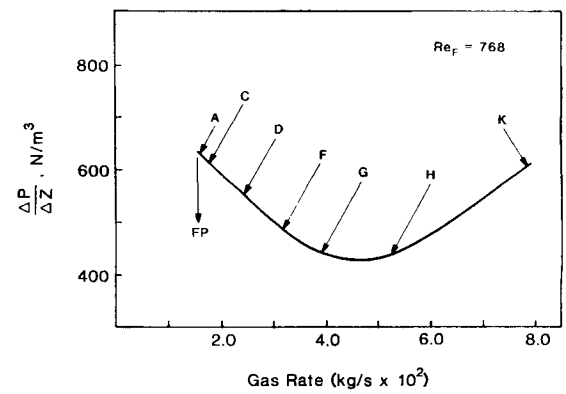

Figure 20. Definition of various flow conditions along a pressure gradient-gas flow rate curve.

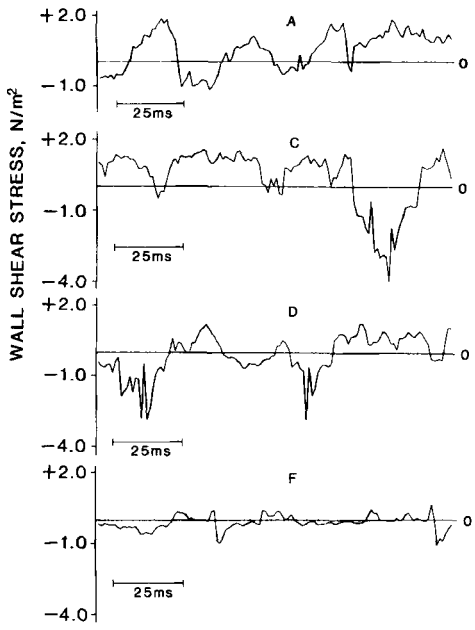

Figure 21. A sequence of wall shear stress traces for increasing gas flow rate.

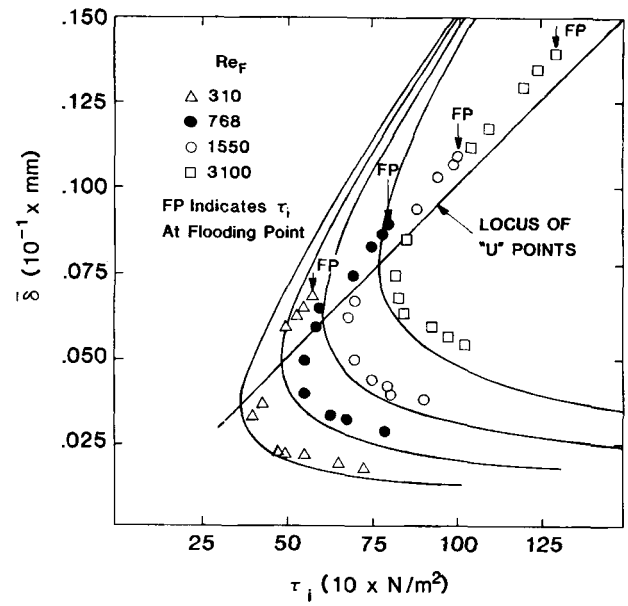

Figure 23. Mean film thickness compared to theory for upflow.

which expresses the momentum balance in the gas phase. Calculated in this way, τ_i represents the sum of the force acting on the interface by the gas and that due to the deposition and entrainment of liquid drops. Recent results by Lopes (1984) show that a significant portion of the total momentum loss can be due to the process of entrainment.

For conditions after flooding and up to the minimum pressure-drop point, the data of Figure 23 are located slightly above the straight line, which is the locus of all states corresponding to zero wall shear stress. There seems to be no way to explain this result except with the concept that the state of the film switches in order to satisfy the two possible solutions, with the resulting mean value of the thickness falling between these two limiting states of the system. The theory was developed for conditions of laminar flow. However the deviations between theory and experiment cannot be ascribed to the possible existence of turbulence in the film. Steady state film thickness under conditions of turbulent flow differ from those for laminar flow by less than 5% over the range of Reynolds numbers. Furthermore the nature of the wall stress measurements is not suggestive of turbulent motion.

Figures 24 and 25 show the measured average values of the wall shear stress vs. the interfacial shear stress. On the same graphs the theoretically calculated values of the wall shear stress assuming nonaccelerating flow are also presented. These have been derived through the following equation:

$$\tau_{w_c} = \rho_L g \delta - \left(-\frac{dP}{dx}\right)\frac{D}{4}. \tag{17}$$

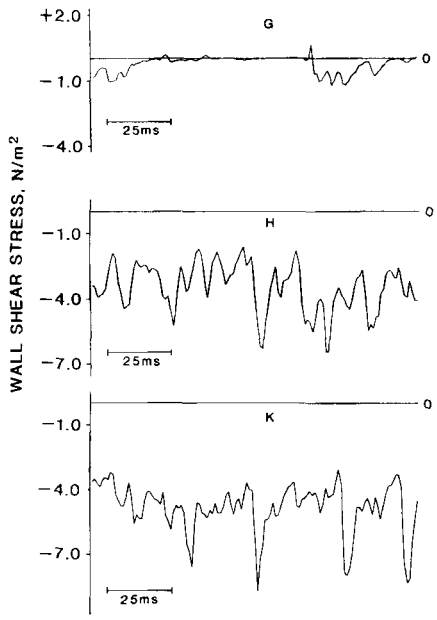

Figure 22. A sequence of wall shear stress traces for increasing gas flow rate.

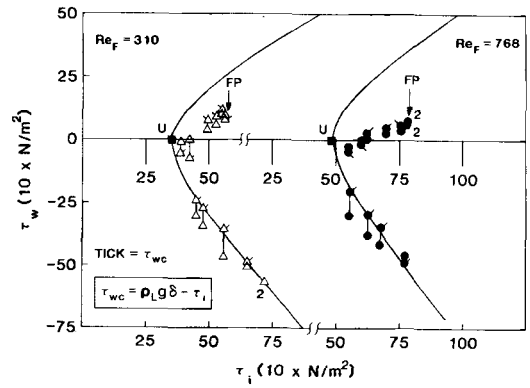

Figure 24. Mean wall shear stress compared to theory for upflow.

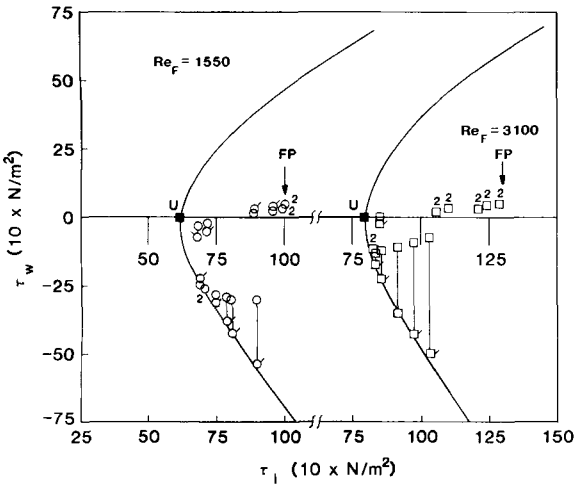

Figure 25. Mean wall shear stress compared to theory for upflow.

The agreement between the experimental and the calculated values is remarkable for the two smallest liquid rates. For the two highest liquid rates there is significant difference between experimental and calculated wall shear stress values only at high gas flow rates. This may be due to the large disturbance or roll waves that exist under these conditions as will be shown below. These cause sufficiently high acceleration that the assumption of no acceleration on which τ_{w_c} is based is no longer valid. Note that the near zero wall stress exists over the entire churn flow region and is not characteristic only of the point of minimum pressure drop.

Figure 26 illustrates a method used to determine if the switching model correctly bounds the observed values of the film thickness in the region where switching is thought to take place. Given the measured value of the mean, and root mean square fluctuation of τ_i for any experiment, it is possible to find from the theoretical solution the corresponding values of the film thickness. These are indicated as thicknesses *2–7* in Figure 26. In addition, the maximum measured τ_i provides an upper and lower bound, thicknesses *1* and *8*. The time trace of film thickness is examined and with these film thickness values *1–8* superimposed. Figures 27 and 28 show four such traces. At low gas flow rates these theoretically determined film thicknesses effectively bound the experimentally observed values, with most of the values falling between *4* and *7*. The fact that the film thickness varies above and below δ_u clearly indicates switching. At high gas flow rates, where the condition is thought to be along branch *UE* (Figure 1), no switching occurs and the time trace oscillates around film thicknesses *1-U*. The film thickness, δ_u, repeatedly appears in all traces and seems to behave as an attractor.

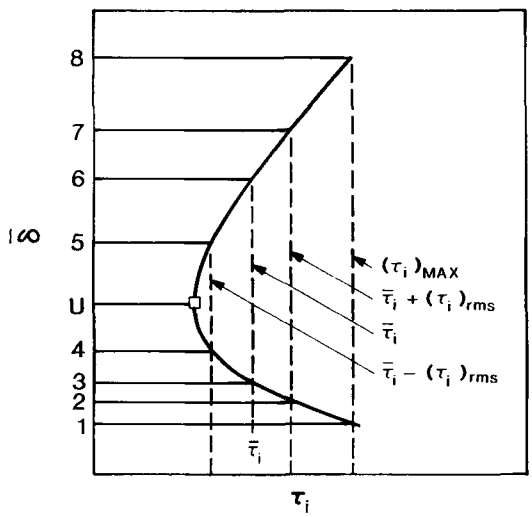

Figure 26. Location of possible steady states.

The existence of large disturbance waves has been recognized in the literature as an important characteristic of vertical upward annular flow at high gas flow rates (Nedderman and Shearer, 1963; Hall-Taylor et al., 1963; Hall-Taylor and Nedderman, 1968; Tomida and Okazaki, 1974). As these authors reported, the characteristic property of the roll waves is their circumferential coherence and their continuity of existence along the tube. Figure 29 compares the normalized crosscovariance of two film thickness signals from sensors located 53 mm apart (Figure 5). The data correspond to six gas rates ranging from conditions near flooding to the highest measured values (Figure 20). The presence of a roll wave moving along the surface at a well-defined propagation velocity would generate a crosscovariance curve with a sharp peak at a negative time

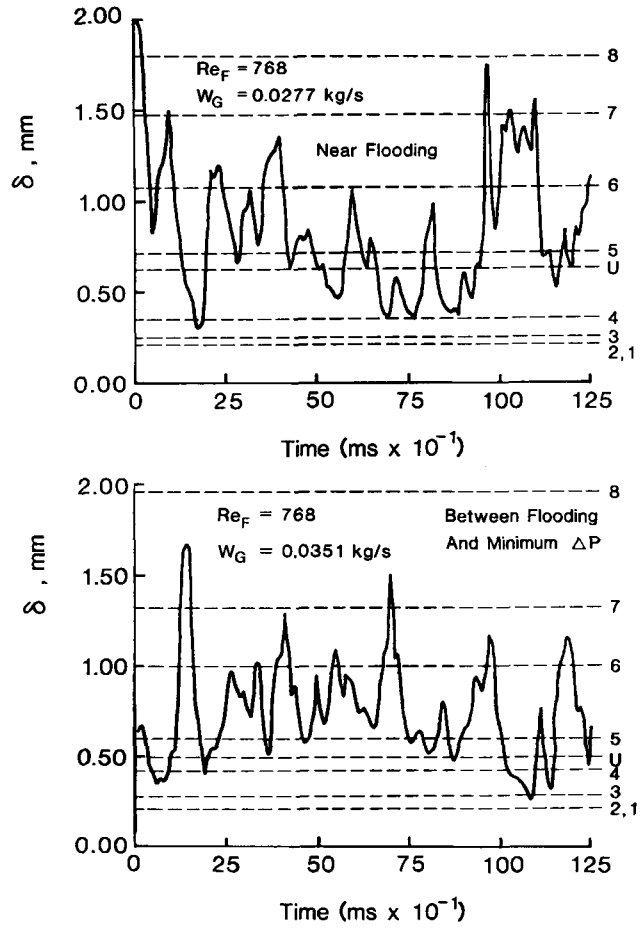

Figure 27. Film thickness traces and some possible states.

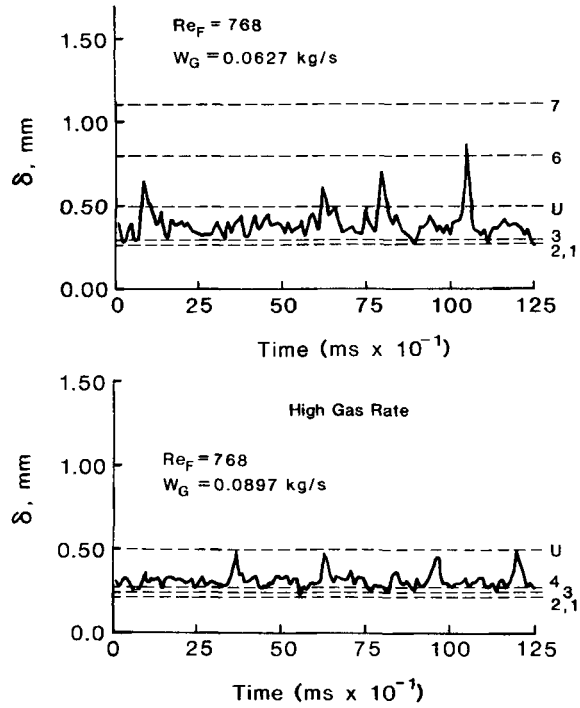

Figure 28. Film thickness traces and some possible states.

delay, as observed for the high gas flow rates (curves *5* and *6*). However, at low gas rates the peak exists at near zero time delay, indicative of the existence of a nonpropagating, stationary process (curves *1* and *2*). This is thought to be the process of switching. As the gas flow rate is increased the peak at nonzero time delay gradually emerges. In fact, more elaborate processing of the data shows that at low gas flow rates both the process of switching and wave motion simultaneously exist, but the switching dominates. As the gas flow rate is increased the wave motion contributes increasingly to the observed structure of the surface until, at high gas flow rates, the switching process is fully suppressed. In order to test this idea the two simultaneous time traces of film thickness were processed to remove large waves. All film thickness levels greater than $\bar{\delta} + \delta_{RMS}$ were replaced in the signal by $\bar{\delta}$. Thus two new film thickness signals were produced that contained only small waves. The crosscovariance of the residual signals is shown in Figure 30 for curves *1–3* of Figure 29. The covariance now displays the symmetrical character expected for stationary random processes, indicating that the curves of Figure 29 are the superposition of those due to the waves and the switching. The existence of a second peak near zero for high gas flow rates can be shown to be due to the spacing of the individual waves in a wave packet.

Typical crosscovariance curves between film thickness and wall shear stress appear in Figure 31. The two detectors were less than 2 mm apart axially and at the same peripheral location. The data at high gas flow rates show a strong peak at negative time delay, precisely as observed for free falling films having pronounced roll waves (Moalem-Maron et al., 1985). The time displacement indicates that the maximum wall shear stress occurs in the rear of the wave. Thus the peak can be associated with roll wave motion. However the data for low gas flow rates show no statistically significant peaks, suggesting again the existence of a stationary process that switches between states of the system.

Figure 32 shows typical results of crosscovariance studies between film thickness and pressure gradient at low and high gas flow rates. Because $\delta \ll D$, interfacial shear stress is linearly related to pressure gradient, as shown in Eq. 16. Thus these curves give insight into the nature of the coupling between τ_i and δ. Strong correlation exists for all flow conditions. However at high flow rates the interfacial shear clearly lags the film thickness in a shape characteristic of wave passage. At low gas flow rates the existence of good correlation over a wide range of time

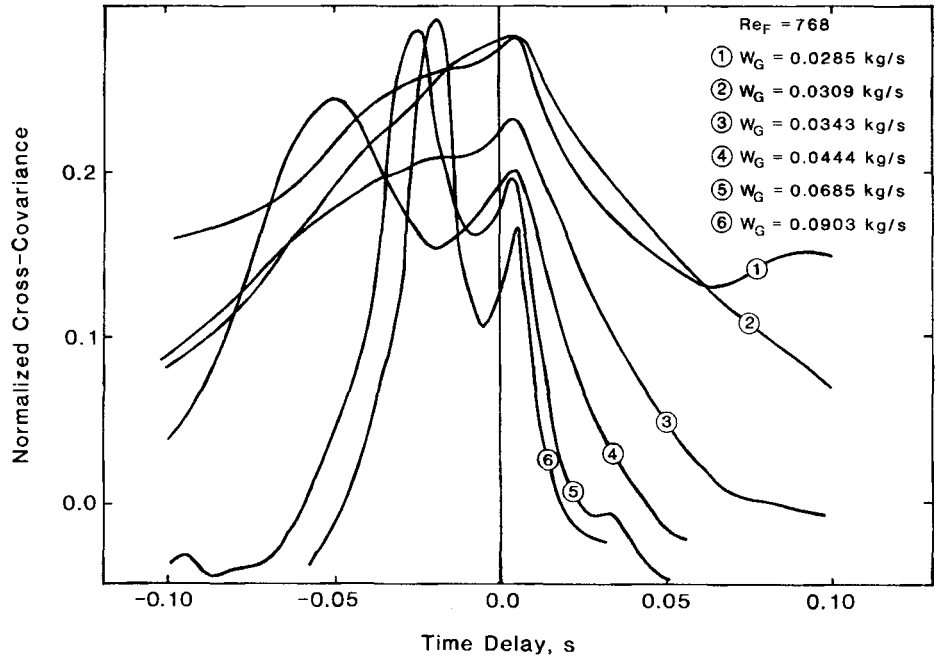

Figure 29. Normalized crosscovariance of two film thickness signals.

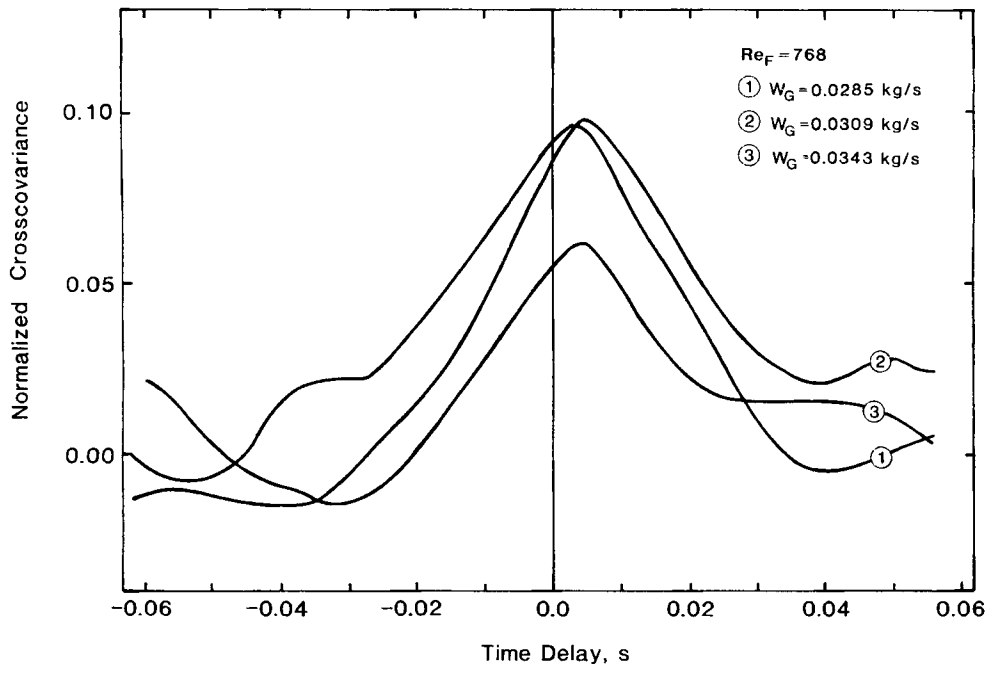

Figure 30. Normalized crosscovariance of two film thickness signals; all thickness levels greater than $\bar{\delta} + \delta_{RMS}$ replaced by $\bar{\delta}$.

delays suggests that a switching process exists with a characteristic dimension in the axial direction greater than the 89 mm spacing of the pressure taps.

The interfacial friction factor can be calculated from

$$f_i = \frac{2\tau_i}{\rho_G(\bar{V}_G - \bar{V}_L)^2} \tag{18}$$

with τ_i calculated from Eq. 16, $\bar{V}_L$ from

$$\bar{V}_L = \frac{W_L}{\rho_L \pi \bar{\delta}(D - \bar{\delta})} \tag{19}$$

and $\bar{V}_G$ from

$$\bar{V}_G = \frac{4W_G}{\rho_G \pi (D - 2\bar{\delta})^2} \tag{20}$$

where W_L, W_G are the measured film and gas mass flow rates.

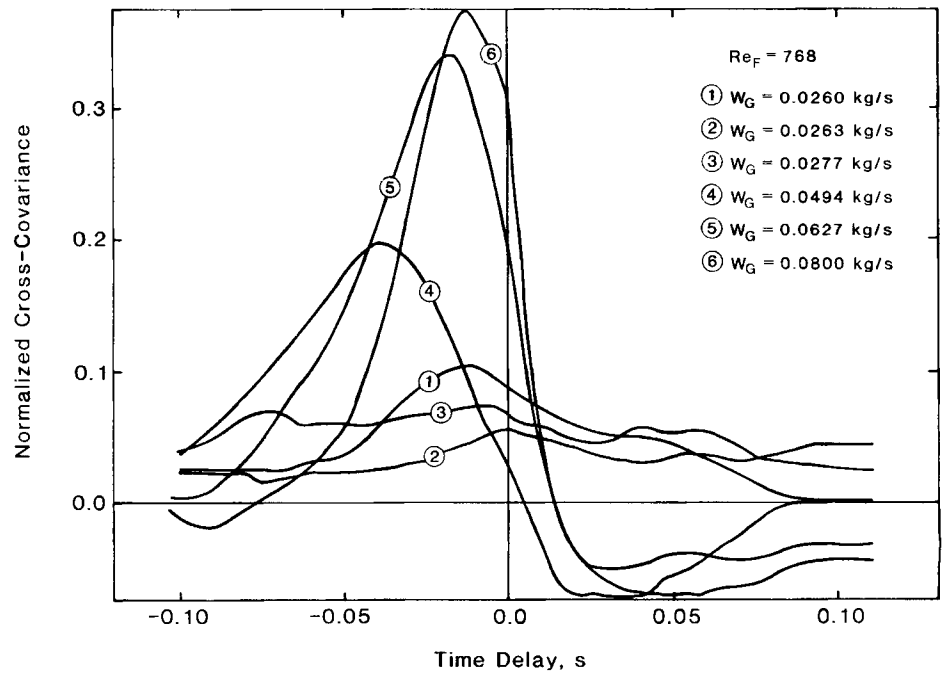

Figure 31. Normalized crosscovariance of film thickness and wall shear stress.

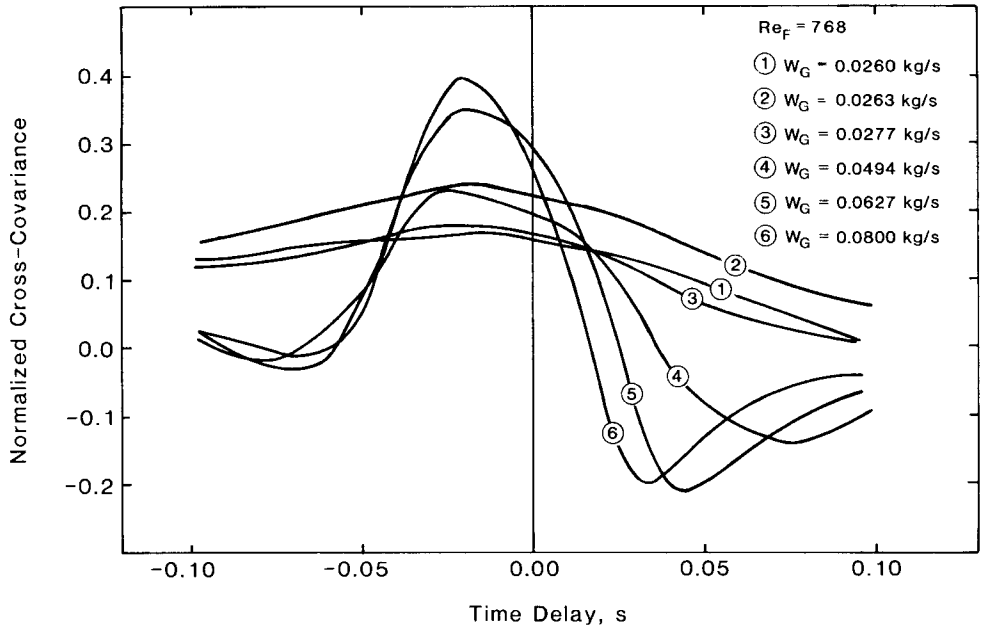

Figure 32. Normalized crosscovariance of film thickness and pressure gradient.

Wallis (1969) suggested that the interfacial friction factor depends uniquely on the ratio of the film thickness to the tube diameter:

$$f_i = 0.005\left[1 + 300\,\frac{\bar{\delta}}{D}\right]. \qquad (21)$$

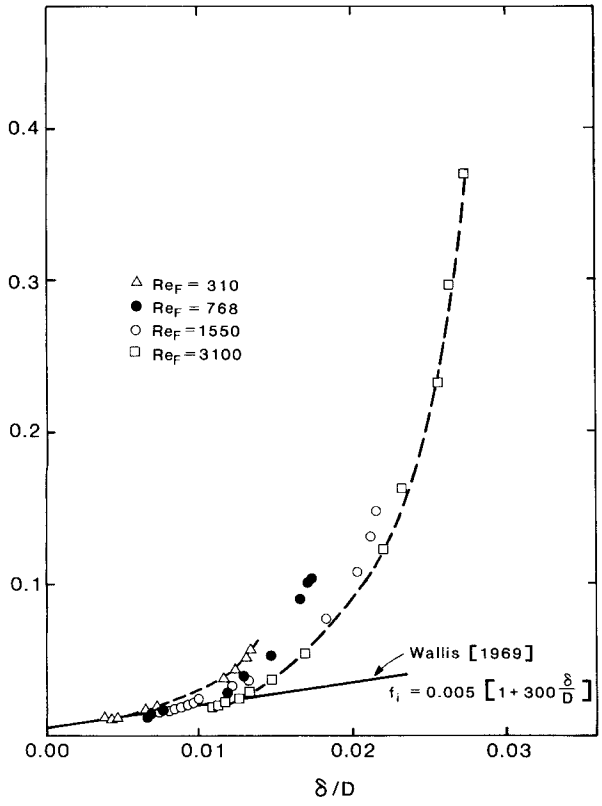

Figure 33. Interfacial friction factor vs. δ/D.

This type of relationship implies a fully rough interface and a unique dependence of roughness on the mean film thickness. Figure 33 compares interfacial friction factors calculated from the data with Eq. 21. It is now evident that this equation reasonably describes the situation for the condition of uniform upflow but is poor in the presence of switching.

Summary

Data are presented for upward annular gas-liquid flow. Analysis of these data in a variety of ways suggests that at low gas flow rates the motion of the interface is controlled by a process of switching between possible steady states of the system as described by Moalem-Maron and Dukler (1984). This condition is one usually designated as churn flow, but bridging of liquid across the pipe as associated with churning does not take place. This switching process can be expected to be accompanied by large dissipative effects. Modeling of the mixing processes associated with heat or mass transfer in the film must be based on the dynamics of switching rather than on wave motion.

At high gas flow rates the interface is characteristic of a sequence of traveling roll waves as described by others. The switching is suppressed.

Acknowledgment

Financial support for this research by the National Science Foundation is gratefully acknowledged.

Notation

c = concentration, kmol/m^3
c_B = bulk concentration, kmol/m^3
D = pipe diameter, m
$\mathcal{D}$ = diffusion coefficient, m^2/s
f_i = interfacial friction factor
g = acceleration of gravity, m/s
G = dimensionless group, Eq. 9
k = mass transfer coefficient, m/s
L = length of the electrochemical probe, m

P = pressure, N/m^2
ΔP = pressure drop, N/m^2
Q_L = liquid film flow rate per unit perimeter, m^2/s
Q_F = liquid feed flow rate per unit perimeter, m^2/s
R_N = dimensionless film thickness, Eq. 9
Re_F = liquid feed Reynolds number, $4Q_F/\nu_L$
u = local velocity in the liquid film, m/s
$\bar{V}_G$ = average gas velocity, m/s
V_G^* = dimensionless gas velocity, $\bar{V}_G\rho_G^{1/2}\,[gD(\rho_L - \rho_G)]^{-1/2}$
$\bar{V}_L$ = average liquid velocity, m/s
W_E = entrainment mass rate, kg/s
W_G = gas mass flow rate, kg/s
W_L = liquid mass flow rate, kg/s
x = axial direction of flow
y = direction normal to flow

Greek letters

δ = film thickness, m
$\bar{\delta}$ = mean film thickness, m
μ = viscosity, kg/ms
ν = kinematic viscosity, m^2/s
ρ = density, kg/m^3
τ_i = interfacial shear stress, N/m^2
τ_w = wall shear stress, N/m^2
ϕ = dimensionless quantity, Eq. 2

Subscripts

c = calculated value
G = gas
L = liquid
N = Nusselt value, corresponding to a smooth free falling film
RMS = root mean square value
u = corresponding to the U state or zero τ_w state

Literature Cited

Brauner, N., and D. Moalem-Maron, "Characteristics of Inclined Thin Films, Waviness and the Associated Mass Transfer," *Int. J. Heat Mass Transfer*, **25**, 99 (1982).

Brown, R. C., P. Andreussi, and S. Zanelli, "The Use of Wire Probes for the Measurement of Liquid Film Thickness in Annular Gas-Liquid Flows," *Can. J. Chem. Eng.*, **56**, 754 (1978).

Buckles, J., T. J. Hanratty, and R. J. Adrian, "Turbulent Flow Over Large-Amplitude Wavy Surfaces," *J. Fluid Mech.*, **140**, 27 (1984).

Cognet, G., M. Lebouche, and M. Sourhar, "Wall Shear Measurements by Electrochemical Probe for Gas-Liquid Two-Phase Flow in Vertical Duct," *AIChE J.*, **30**, 338 (1984).

Dukler, A. E., "The Role of Waves in Two-Phase Flow: Some New Understandings," *Chem. Eng. Education, 1976 Award Lecture*, 108 (1977).

Hall-Taylor, N. S., and R. M. Nedderman, "The Coalescence of Disturbance Waves in Annular Two-Phase Flow," *Chem. Eng. Sci.*, **23**, 551 (1968).

Hall-Taylor, N. S., G. F. Hewitt, and P. M. C. Lacey, "The Motion and Frequency of Large Disturbance Waves in Annular Two-Phase Flow of Air-Water Mixtues," *Chem. Eng. Sci.*, **18**, 537 (1963).

Hewitt, G. F., "Flow Regimes," *Handbook of Multiphase Systems*, G. Hetsroni, ed., Hemisphere, Washington, DC (1982).

Hewitt, G. F., P. M. C. Lacey, and B. Nicholls, "Transition in Film Flow in a Vertical Tube," *Proc. Two-Phase Flow Conf.*, Exeter, England (1965).

Kennedy, J. F., and S. T. Hsu, "Turbulent Flow in Wavy Pipes," *J. Fluid Mech.*, **47**, 481 (1971).

Kvurt, Y. P., et al., "Statistical Nature of the Wave Characteristics of Ascending Two-Phase Film Flow," *Proc. Acad. Sci. USSR*, **243**(6), 1,510 (1978).

Lacey, P. M., and G. F. Hewitt, "Climbing Film Flow," AERE Rept R-3962, Harwell, England (1962).

Lopes, J. C. B., "Droplet Sizes, Dynamics, and Deposition in Vertical Annular Flow," Ph.D. Thesis, Chem. Eng., Univ. Houston (1984).

Malafeev, N. A., V. A. Malyusov, and I. V. Podgornaya, "Investigation of the Hydrodynamics of an Ascending Film-Type Two-Phase Flow in a Flat Channel," *Teoreticheskie Osnovy Khimicheskoi Tekhnologii*, **10**(6), 883 (1976).

Maolem-Maron, D., and A. E. Dukler, "Flooding and Upward Film Flow in Vertical Tubes. II: Speculations on Film Flow Mechanisms," *Int. J. Multiphase Flow*, **10**, 599 (1984).

Maolem-Maron, D., N. Brauner, and A. E. Dukler, "Interfacial Structure of Thin Falling Films: Piecewise Modeling of the Waves," *Physiochem. Hydrodyn.* (1985).

Nedderman, R. M., and C. J. Shearer, "The Motion and Frequency of Large Disturbance Waves in Annular Two-Phase Flow of Air-Water Mixtures," *Chem. Eng. Sci.*, **18**, 661 (1963).

Nicklin, D. J., and B. E. Koch, "A Model of Two-Phase Annular Flow," *Concurrent Gas-Liquid Flow*, Rhodes and Scott, eds., Plenum, New York (1969).

Nikolaev, N. A., et al., "Wave Characteristics for Rising Direct Flow in Air-Water Systems," *Teoreticheskie Osnovy Khimicheskoi Tekhnologii*, **9**(3), 406 (1975).

Orkiszewski, J., "Predicting Two-Phase Pressure Drops in Vertical Pipe," *J. Pet. Tech.*, **19**, 829 (1967).

Reiss, L. P., and T. J. Hanratty, "Measurement of Instantaneous Rates of Mass Transfer to a Small Sink on a Wall," *AIChE J.*, **8**, 245 (1962).

Smith, L., A. Chopra, and A. E. Dukler, "Flooding and Upward Film Flow in Tubes. I: Experimental Studies," *Int. J. Multiphase Flow*, **10**, 585 (1984).

Son, J. C., and T. J. Hanratty, "Velocity Gradients at the Wall for Flow Around a Cylinder at Re from 5×10^3 to 10^5," *J. Fluid Mech.*, **35**, 353 (1969).

Subbotin, V. I., et al., "Integrated Investigation into Hydrodynamic Characteristics of Annular-Dispersed Steam-Liquid Flows," *Proc. 6th Int. Heat Trans. Conf.*, **1**, 327 (1978).

Sutey, A. M., and J. G. Knudsen, "Effect of Dissolved Oxygen on the Redox Method for the Measurement of Mass Transfer Coefficients," *IEC Fundam.*, **6**, 132 (1967).

Tomida, T., and T. Okazaki, "Statistical Character of Large Disturbance Waves in Upward Two-Phase Flow of Air-Water Mixtures," *J. Chem. Eng. Japan*, **7**, 329 (1974).

Wallis, G., *One-Dimensional Two-Phase Flow*, McGraw-Hill, New York (1969).

Whalley, P. B., and G. F. Hewitt, "The Correlation of Liquid Entrainment Fraction and Entrainment Rate in Annular Two-Phase Flow," Rept. AERE-R9187, UKAEA, Harwell, England (1978).

Whalley, P. B., G. F. Hewitt, and P. Hutchinson, "Experimental Wave and Entrainment Measurements in Vertical Annular Two-Phase Flow," Rept. AERE-R7521, Harwell, England (1973).

Zabaras, G., "Studies of Vertical Upward Cocurrent and Countercurrent Annular Gas-Liquid Flows," Ph.D. Thesis, Univ. Houston (1985).

Zielker, D. P., and T. J. Hanratty, "Influence of the Amplitude of a Solid Wavy Wall on a Turbulent Flow. 2: Separated Flows," *J. Fluid Mech.*, **90**, 257 (1979).

Manuscript received Jan. 10, 1985, and revision received Apr. 5, 1985.